

Accelerated generation of holograms with ultra-low memory symmetrically high-compressed look-up table

Yan Yang(杨燕), Jianying Zhu(朱建英), Minyuan Sun(孙敏远), and Yong Bi(毕勇)

Citation: Chin. Phys. B, 2024, 33 (**4**): 044201. DOI: 10.1088/1674-1056/ad1e67
Journal homepage: http://cpb.iphy.ac.cn; http://iopscience.iop.org/cpb

What follows is a list of articles you may be interested in

Generation of orbital angular momentum hologram using a modified U-net

Zhi-Gang Zheng(郑志刚), Fei-Fei Han(韩菲菲), Le Wang(王乐), and Sheng-Mei Zhao(赵生妹)
Chin. Phys. B, 2024, 33 (**3**): 034207. DOI: 10.1088/1674-1056/ad12aa

Bessel—Gaussian beam-based orbital angular momentum holography

Jiaying Ji(季佳滢), Zhigang Zheng(郑志刚), Jialong Zhu(朱家龙), Le Wang(王乐), Xinguang Wang(王新光), and Shengmei Zhao(赵生妹)
Chin. Phys. B, 2024, 33 (**1**): 014204. DOI: 10.1088/1674-1056/acfdff

Multi-channel generation of vortex beams with controllable polarization states and orbital angular momentum

Ziyao Lyu(吕子瑶), Pan Wang(王潘), and Changshun Wang(王长顺)
Chin. Phys. B, 2023, 32 (**12**): 124209. DOI: 10.1088/1674-1056/ace767

Research of NO_2 vertical profiles with look-up table method based on MAX-DOAS

Yingying Guo(郭映映), Suwen Li(李素文), Fusheng Mou(牟福生), Hexiang Qi(齐贺香), and Qijin Zhang(张琦锦)
Chin. Phys. B, 2022, 31 (**1**): 014212. DOI: 10.1088/1674-1056/ac1415

Vertical profile of aerosol extinction based on the measurement of O_4 of multi-elevation angles with MAX-DOAS

Fusheng Mou(牟福生), Jing Luo(雒静), Suwen Li(李素文), Wei Shan(单巍), Lisha Hu(胡丽莎)
Chin. Phys. B, 2019, 28 (**8**): 084212. DOI: 10.1088/1674-1056/28/8/084212

Accelerated generation of holograms with ultra-low memory symmetrically high-compressed look-up table

Yan Yang(杨燕)[1,2], Jianying Zhu(朱建英)[1,2], Minyuan Sun(孙敏远)[1], and Yong Bi(毕勇)[1,†]

[1] *Applied Laser Research Center, Technical Institute of Physics and Chemistry, Chinese Academy of Sciences, Beijing* 100190, *China*
[2] *University of Chinese Academy of Sciences, Beijing* 100049, *China*

(Received 7 November 2023; revised manuscript received 11 January 2024; accepted manuscript online 15 January 2024)

Computer-generated holography technology has been widely applied, and as research in this field deepens, the demand for memory and computational power in small AR and VR devices continues to increase. This paper presents a hologram generation method, i.e., a symmetrically high-compressed look-up table method, which can reduce memory usage by 50%. In offline computing, half of the basic horizontal and vertical modulation factors are stored, halving the memory requirements without affecting inline speed. Currently, its potential extends to various holographic applications, including the production of optical diffraction elements.

Keywords: computergenerated hologram, look-up table, holography

PACS: 42.40.Jv, 42.40.–i **DOI:** 10.1088/1674-1056/ad1e67

1. Introduction

Holographic technology has the capability to reproduce the seven-dimensional light field function completely, which is regarded as the most perfect display technology.[1] It has diverse applications in measurement,[2–7] display,[8–12] storage,[13–15] etc. Computer-generated hologram (CGH) offers lower noise and is unaffected to optical path. CGH is a technique that involves using computational algorithms and numerical methods to generate holographic images. Nowadays, quit a few computer-generated holography techniques have been proposed, including look-up table (LUT),[16–21] wavefront recording plane (WRP),[22–24] ray tracing,[25–27] and deep learning.[28–31] The LUT method involves an efficient calculation technique to synthesize holographic stereograms using precomputed data for rapid processing.[32] The WRP method involves capturing the entire wavefront of light from an object or scene, providing a highly detailed and accurate representation for hologram creation.[22] The ray tracing method simulates light propagation and interaction, effectively capturing and representing occlusions and complex optical phenomena.[33] Deep learning refers to the application of neural networks to learn and simulate the physical processes involved in hologram generation, enabling complex and efficient holographic imaging.[34] Typically, the LUT method is easy to operate and attracts wide attention. In 1997, the LUT method was proposed, which greatly improves the calculation speed, yet it gives rise to the problem of excessive memory consumption which leads to the efficiency of reading out data lower.[16] In 2008, Kim *et al.* proposed N-LUT method, memory reduced to the level of several hundred gigabytes (GBs).[17] In 2009, Pan *et al.* introduced the S-LUT method,[18] this approach effectively minimized the memory usage to several GBs in object space by segregating the storage of horizontal and vertical factors. In 2013, Beijing Institute of Technology introduced the C-LUT method, which only consumed memory in the order of tens of megabytes (MBs).[19] Building on C-LUT, the team proposed an improved AC-LUT method in 2015, reducing memory usage to several MBs.[20] In 2019, the Beijing Institute of Technology further advanced their research and introduced the AHC-LUT method, the memory consumption in physical space was tens of kilobytes (KBs).[21] However, for small near-eye display devices, their memory usage needs reduced further.

In this paper, an ultra-low memory symmetrically high-compressed look-up table (SHC-LUT) method is proposed. The SHC-LUT method is compared with the C-LUT, AC-LUT, AHC-LUT methods on offline computing time, offline memory usage, and inline computing time, demonstrating the advantages of SHC-LUT. To validate the feasibility of proposed method, the simulated and experimental reconstructed images of CGH are performed, the results accord with each other.

2. Proposed method

As shown in Fig. 1, the point source model refers to that the calculated object is regarded as a collection of selfluminous points. The complex amplitude distribution on the hologram plane can be obtained by superimposition of the diffraction image of each point.

The complex amplitude distribution on the hologram

†Corresponding author. E-mail: biyong@mail.ipc.ac.cn

© 2024 Chinese Physical Society and IOP Publishing Ltd

plane is expressed as

$$H(x_{\rm h},y_{\rm h})=\sum_{j=1}^{N}A_j\exp[{\rm i}k(r_j+\varphi_j)], \tag{1}$$

with

$$r_j=\sqrt{(x_{\rm h}-y_j)^2+(y_{\rm h}-y_j)^2+(d-z_j)^2} \tag{2}$$

where $(x_j,\ y_j,\ z_j)$ and A_j represent the coordinates and the amplitude of point j, respectively. N is the number of object point, $k=2\pi/\lambda$ is wave number, and λ is wavelength; φ_j is the initial phase, which can be any number between 0 and 2π; d is the distance between object plane and hologram plane.

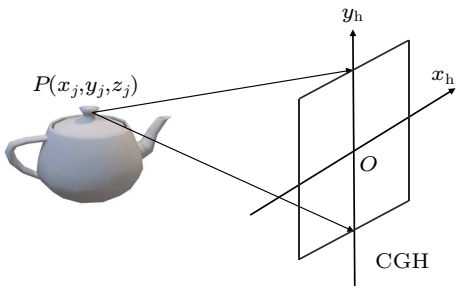


Fig. 1. Schematic diagram of point source model.

In Fresnel diffraction region, according to Ref. [21], the complex amplitude distribution can be rewritten as

$$H(x_{\rm h},y_{\rm h})=\sum_{j=1}^{N}A_j\exp[{\rm i}k(d-z_j)]\times\left\{\exp\left[\frac{(x_{\rm h}-x_j)^2}{2}\right]\times\exp\left[\frac{(y_{\rm h}-y_j)^2}{2}\right]\right\}^{\left(\frac{{\rm i}k}{d-z_j}\right)}. \tag{3}$$

Here, $H(x_{\rm h},x_j)=\exp[(x_{\rm h}-x_j)^2/2]$ is defined as the horizontal modulation factor, $V(y_{\rm h},y_j)=\exp[(y_{\rm h}-y_j)^2/2]$ as the vertical modulation factor, $L_1(z_j)=\exp[{\rm i}k(d-z_j)]$ and $L_2(z_j)={\rm i}k/(d-z_j)$ as the longitudinal and wavelength modulation factor. Then, Eq. (3) can be simply rewritten as

$$H(x_{\rm h},y_{\rm h})=\sum_{j=1}^{N}A_jL_1(z_j)[H(x_{\rm h},x_j)V(y_{\rm h},y_j)]^{L_2(z_j)}. \tag{4}$$

For points falling on the same *xoy* plane, the longitudinal modulation factors $L_1(z_j)$ and $L_2(z_j)$ are the same.

Equation (4) can be rewritten as

$$H(x_{\rm h},y_{\rm h})=\sum_{j_z=1}^{N_z}\left\{\sum_{j_{xy}=1}^{N_{xy}}A_{j_{xy}}\left[H(x_{\rm h},x_j)V(y_{\rm h},y_j)\right]^{L_2(z_j)}\right\}L_1(z_j), \tag{5}$$

where j_z is the sequence number in the 2D plane of 3D object, and j_{xy} is the sequence number of points in the 2D plane.

N_x object points located on the same vertical line in each 2D plane have the same vertical modulation factor $V(y_{\rm h},y_j)$. Thus Eq. (5) can be rewritten as

$$H(x_{\rm h},y_{\rm h})=\sum_{j_z=1}^{N_z}\left\{\sum_{j_y=1}^{N_y}\left[\sum_{j_x=1}^{N_x}A_{j_x}H(x_{\rm h},x_j)^{L_2(z_j)}\right]\times V(y_{\rm h},y_j)^{L_2(z_j)}\right\}L_1(z_j), \tag{6}$$

where j_x and j_y $(j_x=1,2,\ldots,N_x,\ j_y=1,2,\ldots,N_y)$ are the sequence numbers of horizontal and vertical lines of each 2D plane.

$H(x_{\rm h},x_{\rm m})=\exp(x_{\rm h}^2/2)$ is defined as the basic horizontal modulation factor, $V(y_{\rm h},y_{\rm m})=\exp(y_{\rm h}^2/2)$ as the basic vertical modulation factor, with $x_{\rm m},y_{\rm m}=0$. According to the spatial convolution theorem. Other $H(x_{\rm h},x_j)$ can be obtained by simply shifting, $V(y_{\rm h},y_j)$ can also be obtained by shifting.

$$H(x_{\rm h},y_{\rm h})=\sum_{j_z=1}^{N_z}\left\{\sum_{j_y=1}^{N_y}\left[\sum_{j_x=1}^{N_x}A_{j_x}H(x_{\rm h}-x_j,x_{\rm m})^{L_2(z_j)}\right]\times V(y_{\rm h}-y_j,y_{\rm m})^{L_2(z_j)}\right\}L_1(z_j). \tag{7}$$

The basic modulation factors $H(x_{\rm h},x_{\rm m})$, $V(y_{\rm h},y_{\rm m})$ are symmetric about $x_{\rm h}=0$ and $y_{\rm h}=0$, respectively. Thus, $H(x_{\rm h},x_{\rm m})=H_0+{\rm fliplr}(H_0)$, H_0 is half the $H(x_{\rm h},x_{\rm m})$, fliplr is an operator that rotates a 1D array by 180° centered on one end. Similarly, the basic vertical modulation factor $V(y_{\rm h},y_{\rm m})=V_0+{\rm fliplr}(V_0)$. Equation (7) can be rewritten as

$$H(x_{\rm h},y_{\rm h})=\sum_{j_z=1}^{N_z}\left\{\sum_{j_y=1}^{N_y}\left[\sum_{j_x=1}^{N_x}A_{j_x}(H_0+{\rm fliplr}(H_0))^{L_2(z_j)}\right]\times(V_0+{\rm fliplr}(V_0))^{L_2(z_j)}\right\}L_1(z_j). \tag{8}$$

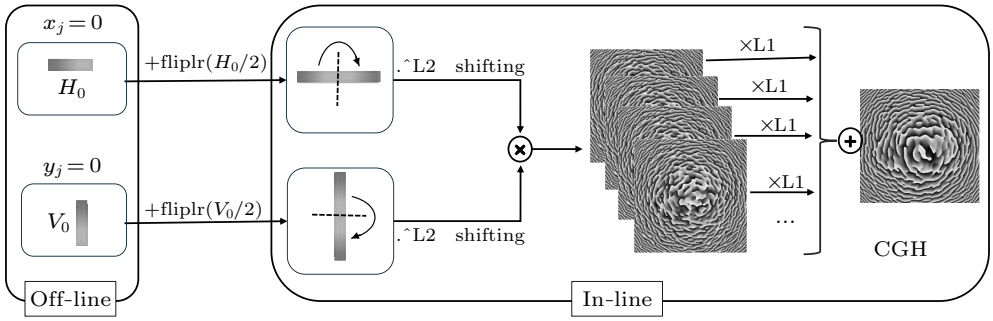


Fig. 2. Diagram of SHC-LUT.

As shown in Fig. 2, the proposed method mainly consists of the following steps. The first step is to compute H_0 and V_0 offline. The second step is to invert H_0 and V_0 to get $H(x_h, x_m)$ and $V(y_h, y_m)$. The third step is to get $H(x_h, x_j)$ and $V(y_h, y_j)$ of each point by shifting, respectively. CGH is obtained by superimposing the complex amplitude distribution of object points.

To ensure the diffraction pattern size of each point can fill the predetermined CGH size after shifting. It is necessary to increase the resolution of the basic modulation factors. If $p \times q$ is the resolution size of the CGH, R_x and R_y are the ratios of the horizontal and vertical sampling intervals of the object space to the horizontal and vertical spacing of the CGH plane pixels, respectively. N_x and N_y are horizontal and vertical resolutions of object space, respectively. Therefore, the resolution of basic modulation factors needs to meet

$$\text{Resolution of } H_0: \ (p + N_x \times R_x)/2,$$
$$\text{Resolution of } V_0: \ (q + N_y \times R_y)/2.$$

To illustrate the simplicity of the proposed method, Table 1 presents the offline computational complexity and memory usage of C-LUT, AC-LUT, AHC-LUT, SHC-LUT. It can be seen that SHC-LUT has the least offline computational complexity and memory usage among four methods. The memory usage of the SHC-LUT method is 50% of the AHC-LUT method. Generally, less memory usage will improve the efficiency of reading data inline.

Table 1. Offline complexity and memory usage of the C-LUT, AC-LUT, AHC-LUT, SHC-LUT methods.

Method	Offline complexity	Memory usage
C-LUT	$p \times N_x + q \times N_y$	$(p \times N_x + q \times N_y)M \times 2$
AC-LUT	$p \times N_x + q \times N_y$	$(p \times N_x + q \times N_y)M$
AHC-LUT	$p + N_x \times R_x + q + N_y \times R_y$	$(p + N_x \times R_x + q + N_y \times R_y)M$
SHC-LUT	$(p + N_x \times R_x + q + N_y \times R_y)/2$	$(p + N_x \times R_x + q + N_y \times R_y)M/2$

3. Algorithm simulation and emulation

To verify the feasibility and advantages of SHC-LUT, four methods are simulated on MATLAB. The object space interval is 10 μm, CGH resolution is 1024×1024, and wavelength of simulation is 638 nm. The four methods run on Intel(R) Core (TM) i5-10400F CPU @ 2.90 GHz.

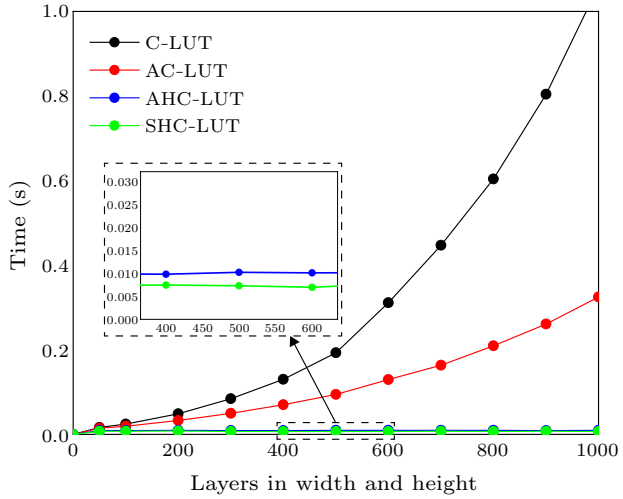


Fig. 3. Comparison of offline computing time by the C-LUT, AC-LUT, AHC-LUT, SHC-LUT methods.

As shown in Fig. 3, the SHC-LUT method has the least offline computing time among the four methods. With the increment of object space width and height, the growth rate of the C-LUT method is the fastest, followed by the AC-LUT method. There is only slight fluctuation in the AHC-LUT and SHC-LUT methods, which fluctuate in millisecond (ms). The offline computing time of the SHC-LUT method keeps several ms, about 30% faster than the AHC-LUT method.

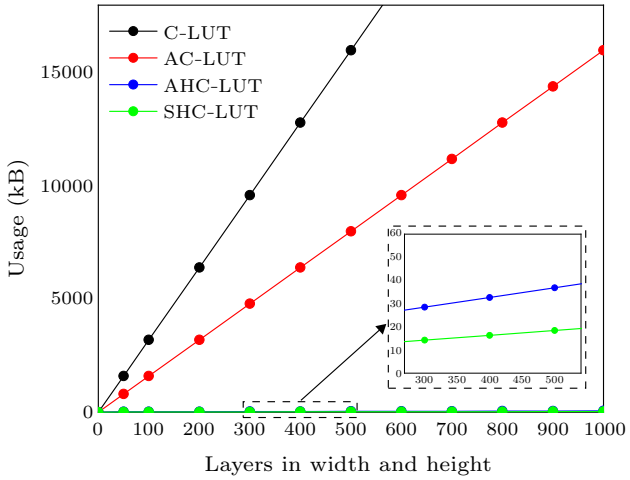


Fig. 4. Comparison of offline memory usage by the C-LUT, AC-LUT, AHC-LUT, SHC-LUT methods.

The memory usage of the four methods is not related to the depth z of the object space.[19–21] Therefore, the width and height of the object space are the main factors of memory usage. From Fig. 4, in the C-LUT method, the memory usage keeps tens of MBs with increment of object space width and height. In the AC-LUT method, the memory usage reduces further but still keeps several MBs. In the AHC-LUT method, the memory usage reduces to tens of KBs. Notably in the SHC-LUT method, as shown in Table 2, the memory usage reduces 50% than the AHC-LUT method. The sampling of width and height is 1000×1000, the memory usage is only 28.875 KBs. Therefore, the proposed method has the least memory usage among the four methods, which accords with the theoretical analysis in Table 1.

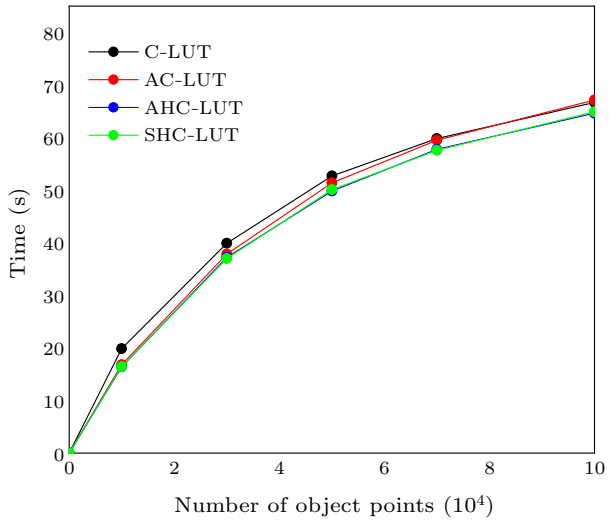


Fig. 5. Comparison of inline computing time by the C-LUT, AC-LUT, AHC-LUT, SHC-LUT methods.

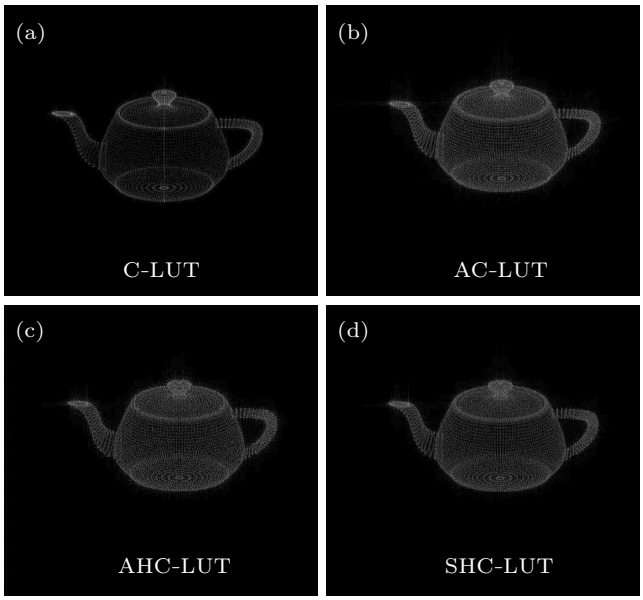


Fig. 6. Numerical simulation of reconstructed results by the C-LUT, AC-LUT, AHC-LUT, SHC-LUT methods.

Table 2. Comparison of memory usage by the C-LUT, AC-LUT, AHC-LU, SHC-LUT methods.

Method	Layers of width and height	Memory usage
C-LUT	500	15.625 MB
	1000	31.25 MB
AC-LUT	500	7.8125 MB
	1000	15.625 MB
AHC-LUT	500	36.86 KB
	1000	57.75 KB
SHC-LUT	500	18.43 KB
	1000	28.875 KB

Random points are selected in the sampling object space of $200 \times 200 \times 200$ for computing inline. As shown in Fig. 5, it can be seen that the inline computing times of the AHC-LUT and SHC-LUT methods are similar, which are less than the C-LUT and AC-LUT methods.

In simulation, the 3D object is reconstructed to verify the feasibility of the proposed method. A teapot object is placed at distance of 300 mm. The hologram plane resolution is 1024×1024, computing the CGH by using the C-LUT, AC-LUT, AHC-LUT, SHC-LUT methods. As shown in Fig. 6, it can be seen that 3D model reconstructed images are accurate by using the AC-LUT, AHC-LUT, SHC-LU methods at the distance of 300 mm. However, the C-LUT method has obvious distortion of reconstructed image accuracy, which can be seen from Fig. 6(a). The reason for reconstruction results variance is that the C-LUT method does not locate in Fresnel diffraction region but in Fraunhofer diffraction region. With the increment of distance, the distortion of the C-LUT method becomes larger.

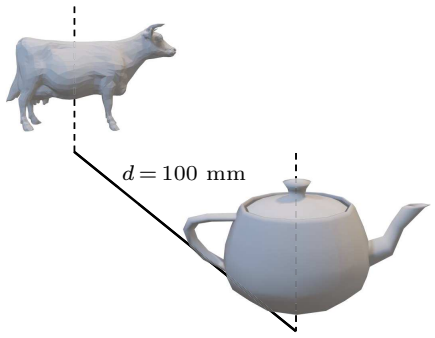


Fig. 7. 3D scenes.

To verify the feasibility of the proposed method further, two 3D objects are placed in a scene located at different distances, as shown in Fig. 7. It can be seen that 3D model reconstructed images are accurate by using the AC-LUT, AHC-LUT, SHC-LUT methods at the distances. The C-LUT method can reconstruct different 3D objects at different distances. Nevertheless, there is obvious distortion of reconstructed size and image accuracy, as shown in Figs. 8(a) and 8(e). The reconstructed size of scenes requires an additional scaling factor to be consistent with the original scene, the image distortion is difficult to solve.

4. Optical experiment

To demonstrate the feasibility of the proposed method, an optical experimental system is established. As shown in Fig. 9. The function of the first part is to expand the light beam to obtain parallel light with uniform energy. In the second part, parallel light irradiates SLM vertically, the phase of the object light wave is reconstructed. However, the phase of the object light wave is mixed with incident parallel light, which affects the viewing quality of the object light wave. The third part is to convert the results of the second step into a spectrum through a Fourier lens. Then, the filter filters out the parallel zero-order light, the clean object phase is observed at corresponding depth.

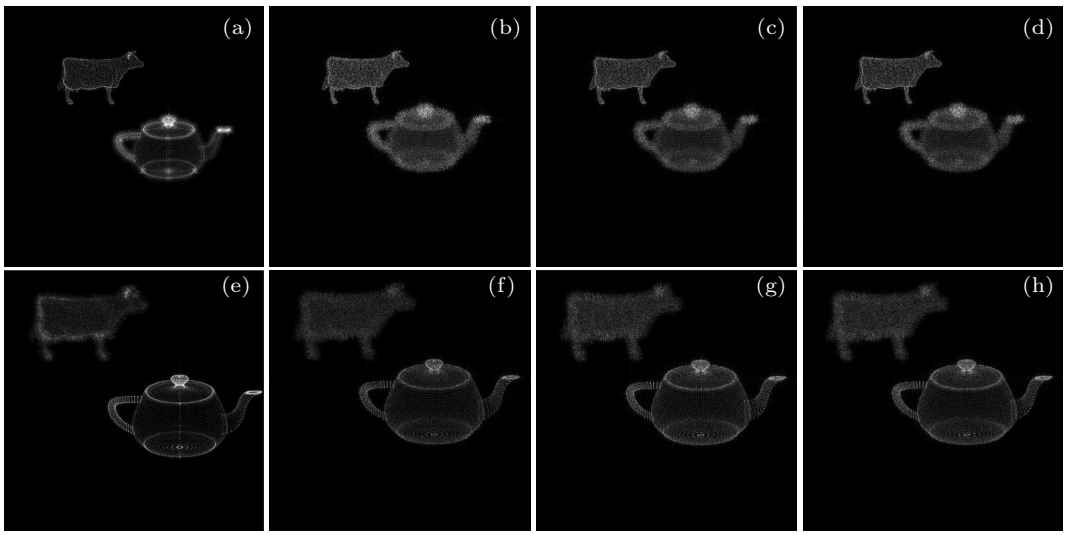


Fig. 8. Numerical simulation of reconstructed results by the C-LUT, AC-LUT, AHC-LUT, SHC-LUT methods. Here, [(a), (e)], [(b), (f)], [(c), (g)], and [(d), (h)] show the reconstructed results by using the C-LUT, AC-LUT, AHC-LUT, and SHC-LUT methods, respectively; [(a)–(d)] and [(e)–(h)] are focused at 300 mm and 400 mm, respectively.

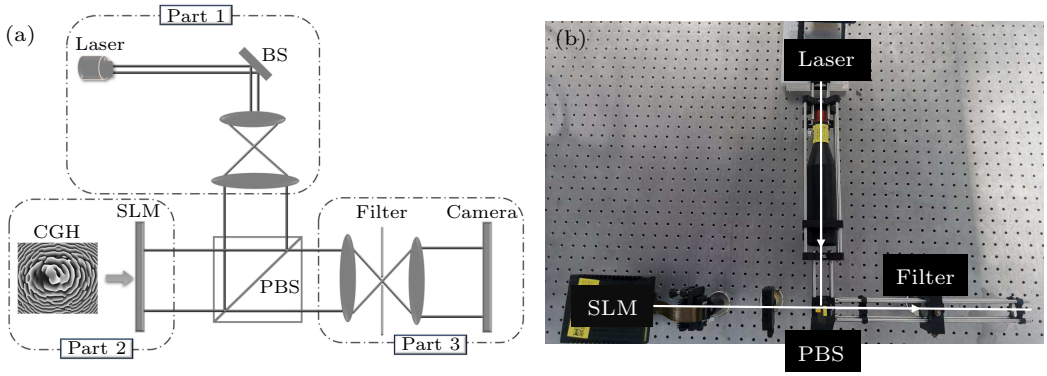


Fig. 9. Optical reconstruction experiment.

The parameters of SLM are listed in Table 3. The wavelength of the reconstructed light is 638 nm, and the reconstructed distance is 300 mm. The C-LUT, AC-LUT, AHC-LUT and proposed SHC-LUT methods are used to obtain the CGH of 3D objects, then, the CGH is loaded on the SLM and reconstructed by an optical experiment.

Table 3. SLM parameters.

Modulation type	phase-only
Liquid crystal type	reflecting
Effective area	15.32 mm × 9.22 mm
Resolution	1024 × 1024
Pixel pitch	3.74 μm
Reflectance	62%–72%
Illuminance (maximum)	2 W/cm^2
Waveband	model dependent
Data interface	HDMI

Figure 10 shows the CGH optical reconstructed images by using the C-LUT, AC-LUT, AHC-LUT, SHC-LUT methods. It can be seen that reconstructed images by using the AC-LUT, AHC-LUT, SHC-LUT method are accurate. However, there is distortion of reconstructed image accuracy for the C-LUT method. As shown in Figs. 10(a). The reconstructed results accord well with the simulation results. Optical experimental results show the accuracy of the SHC-LUT method to achieve 3D reconstructed images.

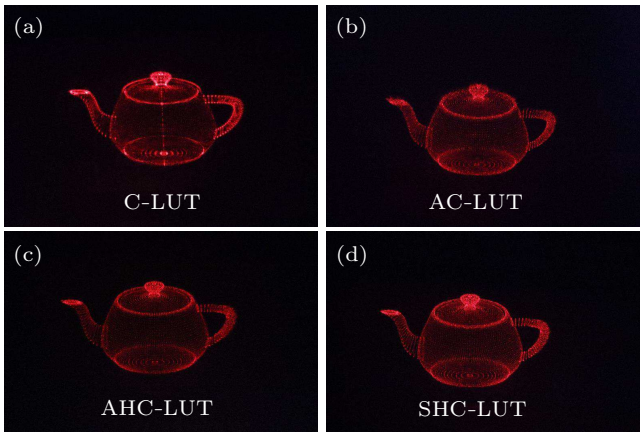


Fig. 10. Optical experimental reconstruction results by the C-LUT, AC-LUT, AHC-LUT, SHC-LUT methods.

From Fig. 11, it can be seen that 3D model reconstructed images and reconstructed size are accurate by using the AC-LUT, AHC-LUT, SHC-LUT methods at respective distance.

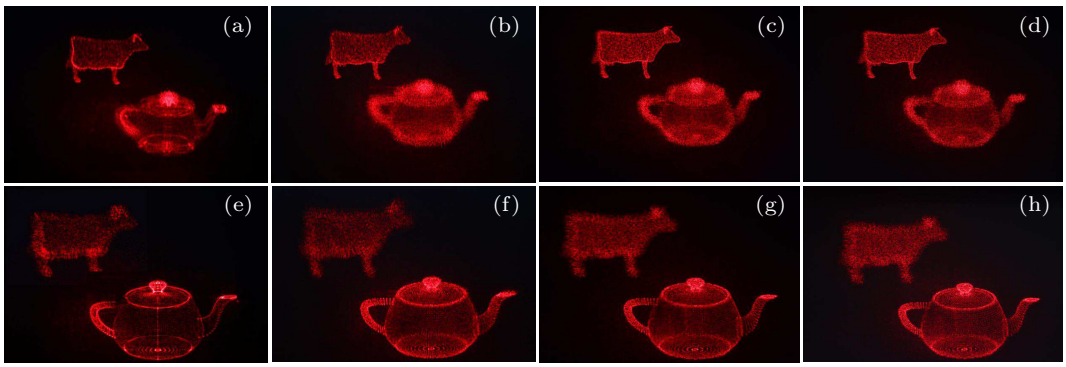


Fig. 11. Optical experimental reconstruction results focused on different distance. Here, [(a), (e)], [(b), (f)], [(c), (g)], and [(d), (h)] show the reconstructed results by using the C-LUT, AC-LUT, AHC-LUT, and SHC-LUT methods, respectively; [(a)–(d)] and [(e)–(h)] are focused at 300 mm and 400 mm, respectively.

The reconstructed distance of the C-LUT method is exact. Nevertheless, there is distortion of reconstructed size and image accuracy. As shown in Figs. 11(a) and 11(e), an additional scaling factor is added to the program to control the size of the reconstructed scene.

5. Conclusions

This paper proposes a symmetrically high-compressed LUT method of CGH in Fresnel diffraction region. In offline computing, after separating the longitudinal and wavelength modulation factors, the basic vertical and horizontal modulation factors are compressed to 1D arrays, respectively. Moreover, the two 1D arrays are symmetric, which verify that storing half the arrays data is feasible. Therefore, the proposed method has the least memory usage which improves the efficiency of reading data. In inline computing, other horizontal and vertical modulation factors of object points can be obtained by simply shifting the basic horizontal and vertical modulation factors without sacrificing the speed. To verify the feasibility of the proposed method, simulated and experimental reconstructed images of 3D objects are performed. Simulations and optical experiments results accord well with each other. The proposed method alleviates the distortion of the C-LUT method, improves the inline speed of the AC-LUT method, reduces the memory usage 50% of the AHC-LUT method without sacrificing the inline speed. Our next work is to combine the proposed method on GPU with optical waveguide near-eye display devices. For small holographic near eye display devices, the proposed method has great potential for its small memory usage requirement. In addition, the proposed method is expected to be used in the fields of optical waveguide fabrication.

Acknowledgments

Project supported by the National Natural Science Foundation of China (Grant No. 62205350), the Special Project of Central Government Guiding Local Science and Technology Development in Beijing 2020 (Grant No. Z20111000430000), and the Guangxi Nanning Key R&D Program (Grant No. 20233067).

References

[1] Zuo Chao and Chen Qian 2022 *Infr. Laser Engin.* **51** 20220110
[2] De Oliveira I and Miyazawa K 2023 *Opt. Commun.* **546** 129764
[3] Song Q, Xi J, Wang S, *et al.* 2023 *Opt. Commun.* **546** 129801
[4] Sirohi R 2022 *Light: Adv. Manufact.* **3** 35
[5] Kozacki T, Mikuła-Zdańkowska M, Martinez-Carranza J and Idicula M S 2021 *Opt. Express* **29** 21965
[6] Wang Y, Zhang X, Zhao Q, Yao Y, Yan P and Wang B 2022 *Chin. Phys. B* **31** 034202
[7] Boudaoud F and Lemerini M 2015 *Chin. Phys. B* **24** 075205
[8] Xiao D, Li X, Liu S J and Wang Q H 2018 *Opt. Commun.* **410** 488
[9] Kim Y H, Choi K H, Baek I B, *et al.* 2023 *Opt. Commun.* **546** 129818
[10] Choo H G, Kozacki T, Zaperty W, Chlipala M, Lim Y and Kim J 2019 *Appl. Opt.* **58** G96
[11] Yuan Y, Sun M Y, Bi Y, Gao W N, Zhang S and Zhang W P 2021 *Chin. Phys. B* **30** 014209
[12] Gao H Y, Yao Q X, Liu P, *et al.* 2016 *Chin. Phys. B* **25** 094203
[13] Gao H Y, Liu P, Zeng C, Yao Q X, Zheng Z, Liu J, Zheng H, Yu Y J, Zeng Z X and Sun T 2016 *Chin. Phys. B* **25** 094205
[14] Das B, Joseph J and Singh K 2009 *Opt. Commun.* **282** 2147
[15] Judeinstein P, Oliveira P W, Krug H and Schmidt H 1997 *Adv. Mater. Opt. Electron.* **7** 123
[16] Lucente M E 1993 *J. Electron. Imaging* **2** 28
[17] Kim S C and Kim E S 2008 *Appl. Opt.* **47** D55
[18] Pan Y, Xu X, Solanki S, *et al.* 2009 *Opt. Express* **17** 18543
[19] Jia J, Wang Y, Liu J, *et al.* 2013 *Appl. Opt.* **52** 1404
[20] Gao C, Liu J, Li X, *et al.* 2015 *Opt. Express* **23** 33194
[21] Pi D, Liu J, Kang R, Zhang Z and Han Y 2019 *Opt. Express* **27** 28410
[22] Shimobaba T, Masuda N and Ito T 2009 *Opt. Lett.* **34** 3133
[23] Hasegawa N, Shimobaba T, Kakue T and Ito T 2017 *Appl. Opt.* **56** A97
[24] Arai D, Shimobaba T, Murano K, Endo Y, Hirayama R, Hiyama D, Kakue T and Ito T 2015 *Opt. Express* **23** 1740
[25] Blinder D, Chlipala M, Kozacki T and Schelkens P 2021 *Opt. Lett.* **46** 2188
[26] Sun M, Yuan Y, Bi Y, Zhu J, Zhang S and Zhang W 2020 *Laser and Optoelectron. Prog.* **57** 240901 (in Chinese)
[27] Wang Y, Chen Z, Sang X, Li H and Zhao L 2018 *Opt. Commun.* **410** 768
[28] Shi L, Li B, Kim C, Kellnhofer P and Matusik W 2021 *Nature* **591** 234
[29] Ishii Y, Shimobaba T, Blinder D, Birnbaum T, Schelkens P, Kakue T and Ito T 2022 *Appl. Phys. B* **128** 22
[30] Zhang Y, Zhang M, Liu K, He Z and Cao L 2022 *Appl. Sci.* **12** 8568
[31] Horisaki R, Nishizaki Y, Kitaguchi K, Saito M and Tanida J 2021 *Appl. Opt.* **60** A323
[32] Wang Z, Lv G, Feng Q, Wang A and Ming H 2019 *Appl. Opt.* **58** A41
[33] Liu S, Wei H, Li N, Liu Z and Zhang J 2019 *Opt. Commun.* **443** 76
[34] Shimobaba T, Blinder D, Birnbaum T, Hoshi I, Shiomi H, Schelkens P and Ito T 2022 *Front. Photon.* **3** 854391